



# Toward biomass-based single-atom catalysts and plastics: Highly active single-atom Co on N-doped carbon for oxidative esterification of primary alcohols

Hua Zhou<sup>a,1</sup>, Song Hong<sup>b,1</sup>, Hao Zhang<sup>c,d,1</sup>, Yongting Chen<sup>e,1</sup>, Huanghui Xu<sup>a</sup>, Xueke Wang<sup>a</sup>, Zheng Jiang<sup>c,f,\*\*</sup>, Shengli Chen<sup>e,\*\*</sup>, Yun Liu<sup>a,\*</sup>

<sup>a</sup> Beijing Key Laboratory of Bioprocess, College of Life Science and Technology, Beijing University of Chemical Technology, Beijing 100029, China

<sup>b</sup> Center for Instrumental Analysis, Beijing University of Chemical Technology, Beijing 100029, China

<sup>c</sup> Shanghai Synchrotron Radiation Facility, Shanghai Institute of Applied Physics, Chinese Academy of Sciences, Shanghai 201204, China

<sup>d</sup> University of Chinese Academy of Sciences, Beijing 100049, China

<sup>e</sup> College of Chemistry and Molecular Sciences, Wuhan University, Wuhan 430072, China

<sup>f</sup> Shanghai Synchrotron Radiation Facility, Zhangjiang Lab, Shanghai Advanced Research Institute, Chinese Academy of Science, Shanghai 201210, China

## ARTICLE INFO

### Keywords:

Single-atom catalysts  
Biomass conversion  
Metal-lignin complexes  
Oxidative esterification  
Renewable plastics

## ABSTRACT

Supported single-atom catalysts (SACs) have attracted much attention as their advantageous performances in heterogeneous catalysis. Here, we report a general synthesis approach to produce SACs on nitrogen-doped carbon (M SAs-N@C, where M = Fe, Co, Ni, Cu) by engineering bioinspired metal-lignin coordination complexes. The Co SAs-N@C catalyst shows extraordinary reactivity for the oxidative esterification of primary alcohols via aldehyde intermediates, achieving a high turnover frequency (TOF, 55.6 mol<sub>methyl benzoate</sub> mol<sub>Co</sub><sup>-1</sup> h<sup>-1</sup>) for benzyl alcohol, which is approx. 18 times of Co nanoparticles. Experiments and theoretical calculations reveal that the atomically dispersed Co species in Co SAs-N@C are active sites for this reaction. As a proof-of-concept, we demonstrate an integrated biorefinery that lignin-based catalyst enables the effective transformation of carbohydrate-derived furans into building block of plastics and fragrance. Our technique not only provides a facile, low-cost and scalable method to atomically dispersed catalysts but also opens new avenue toward lignin valorization and biomass economy.

## 1. Introduction

Atomically dispersed transition metal species (i.e. clusters and single-atoms) supported on solid supports have attracted much attention as their extraordinary performances in industrial reactions, [1] environmental catalysis [2,3], and emerging catalytic processes [4]. In particular, SACs on carbon support are versatile catalysts in electrochemistry [4–6], organic synthesis, [1,7,8], catalytic degradation [9], etc., because of the high reactivity of coordinatively unsaturated metal centers and conductivity and durability of carbon. However, the large-scale fabrication of such SACs is still of great challenge because of the high surface free energy of single atoms [10,11].

Wet-chemistry strategies are promising for the industrial scale production of SACs. [12] However, in traditional wet-chemistry

methods, the aggregation of free metal precursors during drying process often result in the formation of large nanoparticles in post-treatment [12,13]. Creating strong interactions (such as, coordination effect, electrostatic adsorption) between atomic metal precursors and supports or organic ligands in improved wet-chemistry approaches have been demonstrated to be effective for the synthesis of SACs [14–17]. Small molecular ligands, e.g. 2-methyl imidazole, 1,10-phenanthroline, have been extensively studied to hold the metal atoms in the starting materials of carbonaceous SACs [14,16]. Despite these well-developed techniques, the development of cost-effective and scalable SACs for practical application is still of challenging [18,19].

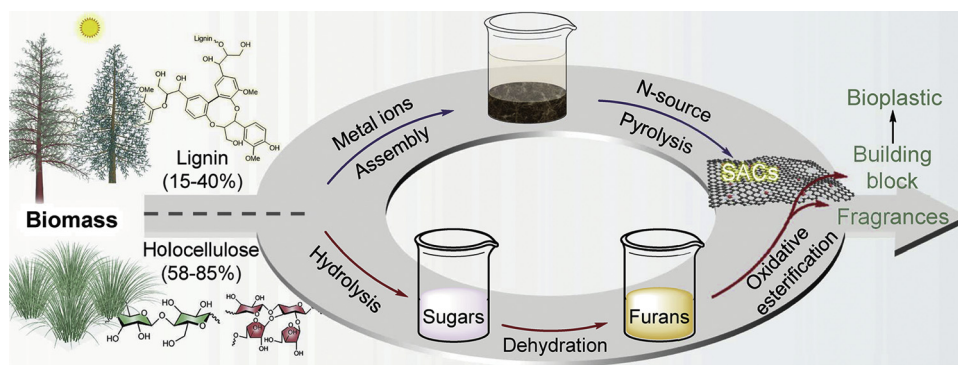
Inspired by the natural iron-catechol complexes in marine mussels, [20] we recently found that lignin can coordinated with transition metal ions such as Mn<sup>II</sup> and Co<sup>II</sup> owing to its intrinsic phenolic

\* Corresponding author at: Beijing Key Laboratory of Bioprocess, College of Life Science and Technology, Beijing University of Chemical Technology, Beijing 100029, China.

\*\* Corresponding authors.

E-mail addresses: [jiangzheng@sinap.ac.cn](mailto:jiangzheng@sinap.ac.cn) (Z. Jiang), [slchen@whu.edu.cn](mailto:slchen@whu.edu.cn) (S. Chen), [liuyunprivate@sina.com](mailto:liuyunprivate@sina.com) (Y. Liu).

<sup>1</sup> These authors contributed equally.



**Scheme 1.** Overview of the integrated biorefinery. Engineering metal-lignin (M-L) complexes to single-atom catalysts (SACs) for the upgrading of carbohydrate-derived furans.

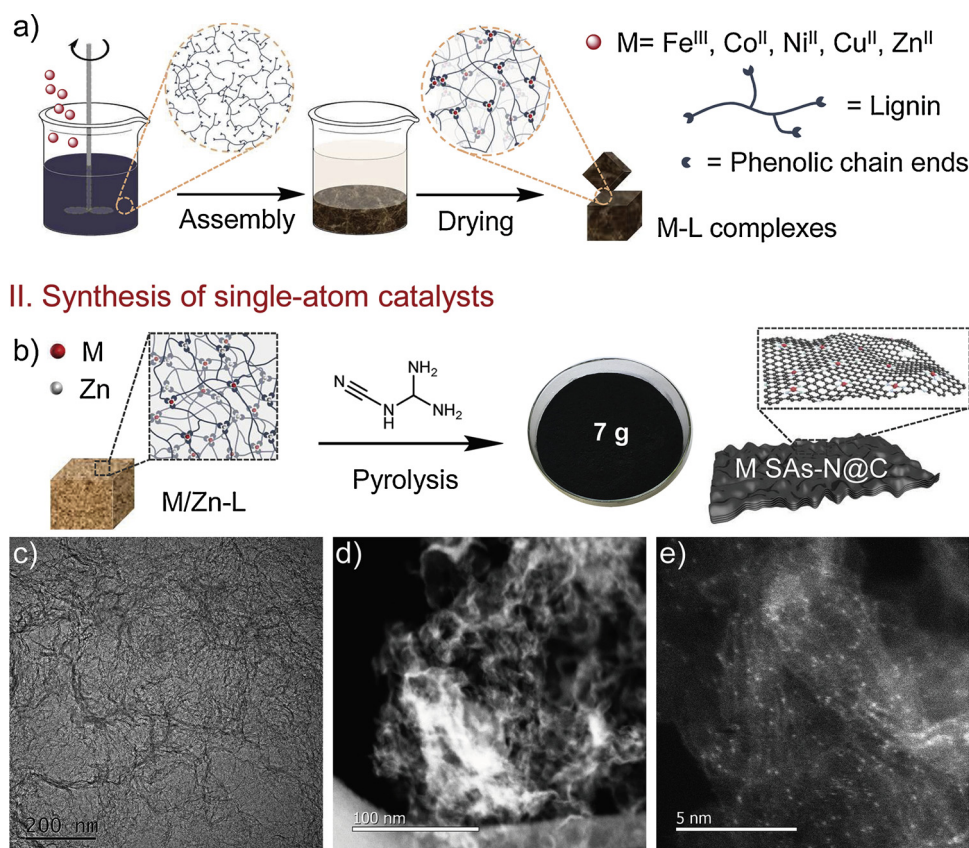


**Fig. 1.** Strategy for the synthesis of SACs. a) Schematic illustration of the assembly process of metal-lignin (M-L) complexes. b) Diagram for the preparation of M SAs-N@C. c) TEM and d, e) HAADF-STEM images of Co SAs-N@C.

structure. [21] Herein, we demonstrate the assembly of metal-lignin (M-L) complexes for producing SACs supported on nitrogen-doped carbon (M SAs-N@C, M = Fe, Co, Ni, Cu). The atomic dispersion of metal population in M SAs-N@C materials is confirmed by high-angle annular dark-field scanning transmission electron microscope (HAADF-STEM) and x-ray absorption fine structure spectroscopy (XAFS). Specifically, the atomically dispersed Co-N<sub>x</sub> species on Co SAs-N@C catalyst are disclosed to be responsible for oxidative esterification of primary alcohols and aldehydes by experiments and density functional theory (DFT) calculations. Furthermore, we propose a strategy for full lignocellulose utilization that holocellulose derived oxygenates are converted into valuable building block and fragrance using lignin-based Co SAs-N@C catalyst (Scheme 1).

## 2. Experimental section

### 2.1. Materials

Alkaline lignin (product No. 471003), dicyandiamide (99%), benzyl alcohol (≥99%), benzaldehyde (≥99%), methyl benzoate (99%), 5-(Hydroxymethyl)furfural (≥99%), furfural (99%), and anisole (analytical standard) were purchased from Sigma-Aldrich. Furan-2,5-dicarbaldehyde, diethyl furan-2,5-dicarboxylate, dimethyl furan-2,5-dicarboxylate, and 2,5-furandicarboxylic acid were purchased from Suzhou Guide Fine Materials Co. Ltd.. Iron nitrate, cobalt nitrate, nickel nitrate, cupric nitrate, and zinc nitrate were analytical purity and purchased from Tianjin North Fine Chemicals Development Co., Ltd. Methanol, ethanol, ethyl acetate, sulfuric acid and ammonia (25%) were of analytical purity and purchased from Beijing Chemical Works.

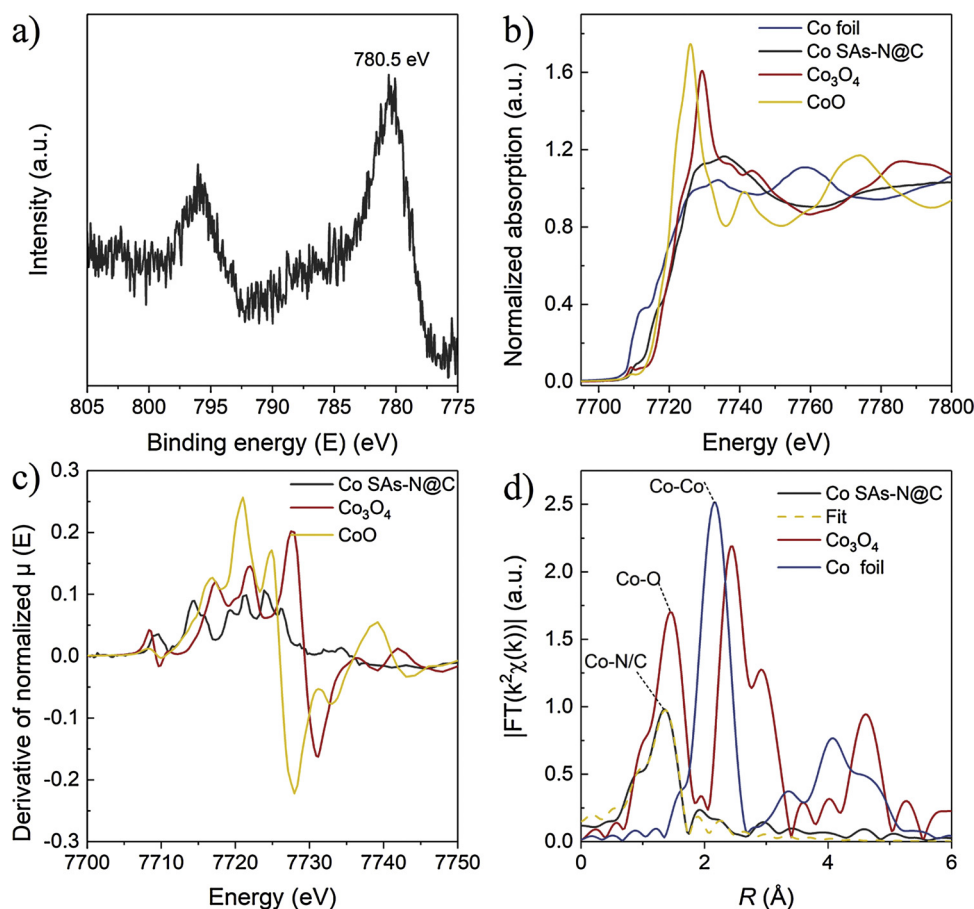


**Fig. 2.** a) Co2p XPS spectrum of Co SAs-N@C. b) XANES spectra and c) derivative of normalized XANES of Co SAs-N@C, CoO and Co<sub>3</sub>O<sub>4</sub>. d) EXAFS spectra and fitting curve of Co SAs-N@C and reference samples.

**Table 1**

K-edge EXAFS fitting parameters of Fe, Co, Ni and Cu within different catalysts.

Sample	shell	N	R (Å)	$\Delta E_0$ (eV)	$\sigma^2(10^{-3} \text{ Å}^2)$	R-factor
Fe SAs-N@C	Fe-C	$1.0 \pm 0.2$	$1.80 \pm 0.01$	$-6.5 \pm 0.5$	$6.9 \pm 3.0$	0.004
	Fe-O	$1.7 \pm 0.1$	$1.89 \pm 0.01$	$-6.5 \pm 0.5$	$2.9 \pm 0.6$	
	Fe-N	$3.0 \pm 0.3$	$2.02 \pm 0.01$	$-6.5 \pm 0.5$	$6.9 \pm 1.2$	
Co SAs-N@C	Co-C	$1.0 \pm 0.5$	$1.75 \pm 0.02$	$10.3 \pm 1.1$	$9.5 \pm 8.3$	0.005
	Co-N	$2.9 \pm 0.2$	$1.86 \pm 0.01$	$10.3 \pm 1.1$	$2.5 \pm 1.0$	
Ni SAs-N@C	Ni-C	$1.0 \pm 0.3$	$1.75 \pm 0.01$	$-8.8 \pm 0.7$	$6.5 \pm 3.5$	0.003
	Ni-N	$3.0 \pm 0.2$	$1.87 \pm 0.01$	$-8.8 \pm 0.7$	$2.9 \pm 0.8$	
Cu SAs-N@C	Cu-C	$0.8 \pm 0.3$	$1.78 \pm 0.02$	$3.4 \pm 1.0$	$7.4 \pm 5.6$	0.006
	Cu-N	$3.0 \pm 0.3$	$1.91 \pm 0.01$	$3.4 \pm 1.0$	$6.1 \pm 1.6$	

Notes: N, coordination numbers; R, the internal atomic distance;  $\Delta E_0$ , the edge-energy shift;  $\sigma^2$ , Debye-Waller factor.

[BMIM][Cl] was bought from Shanghai Cheng Jie Chemical Co. Ltd. All reagents were used without any further purification.

## 2.2. Synthesis of Co SAs-N@C

Typically, 8 g lignin was dissolved in 1000 mL deionized water with mechanical stirring to form black lignin solution. Metal ions solution with  $\text{Co}(\text{NO}_3)_2 \cdot 6\text{H}_2\text{O}$  (8 mmol) and  $\text{Zn}(\text{NO}_3)_2 \cdot 6\text{H}_2\text{O}$  (40 mmol) was added into the lignin solution and kept stirring for 1 h. Finally, the Co/Zn-L complex was separated through centrifugation after ~12 h of aging and dried at 80 °C overnight. The as-obtained Co/Zn-L complex was homogeneously mixed with ten times weight of dicyandiamide by grinding in a mortar. The mixture powder was annealed at 550 °C for 1 h and then at 1000 °C for 1 h in a tube furnace under an argon atmosphere with the flow rate of 70 mL/min. After cooling to room

temperature, the obtained material was grinded for test.

## 2.3. Characterizations

X-ray diffraction (XRD) was recorded on a Rigaku Ultima IV diffractometer at 40 mA and 40 kV using Cu K $\alpha$  radiation ( $\lambda = 1.54$ ,  $10^\circ \text{ min}^{-1}$  from 5 to  $90^\circ$ ). X-ray photoelectron spectroscopy (XPS) was performed on a ThermoFisher Scientific ESCALAB 250XI using monochromated Al K $\alpha$  source (150 W, 500  $\mu\text{m}$ ). SEM images with EDX mapping were collected on a Hitachi S4700 equipped with an energy dispersive X-ray (EDX) spectroscopy at 10 kV. High angle annular dark-field scanning transmission electron microscopy (HAADF-STEM) images were acquired on JEOL JEM-ARM200 F at 200 kV. Raman spectra were recorded on a Renishaw inVia Micro-Raman Spectroscopy System equipped with CCD detector at 633 nm. TGA analysis was



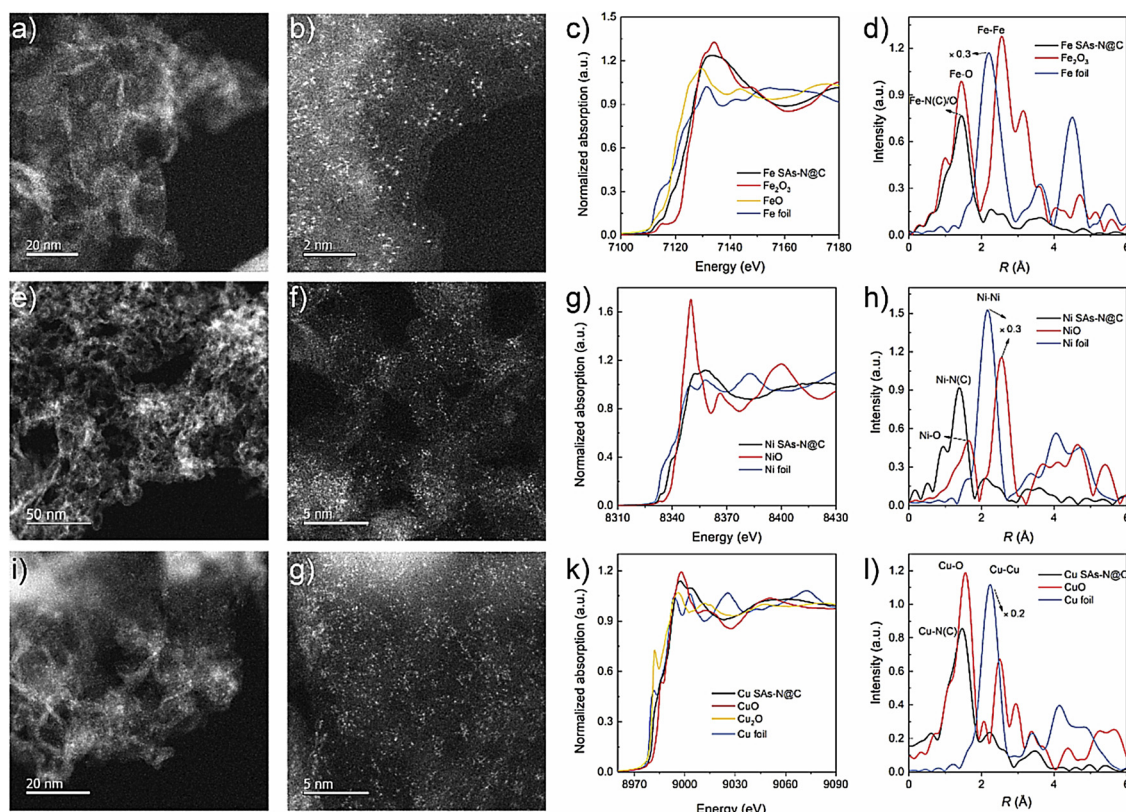
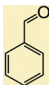
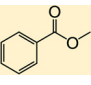


Fig. 3. HAADF-STEM images, XANES and EXAFS spectra of M SAs-N@C. a–d) Fe SAs-N@C, e–h) Ni SAs-N@C, and i–l) Cu SAs-N@C.

Table 2

Comparison of the catalytic activity of M SAs-N@C for oxidative esterification of benzyl alcohol.<sup>a</sup>

Catalyst	C (%)	Y (%)	
			
Fe SAs-N@C	11.75	9.94	0.25
Co SAs-N@C	99.8	1.4	97.5
Ni SAs-N@C	6.4	5.16	0.46
Cu SAs-N@C	9.62	7.66	–

<sup>a</sup> Reaction conditions: 0.5 mmol benzyl alcohol, M SAs-N@C catalyst (contain 12.5 μmol metal), 5 mL CH<sub>3</sub>OH, O<sub>2</sub> balloon (1 bar), 60 °C, 3 h. C: conversion, Y: yield.

performed on a SHIMADU DTG-60A thermoanalyzer under flowing nitrogen at 50 mL min<sup>-1</sup>, the temperature was ranged from 40 to 1000 °C at the heating rate of 10 °C min<sup>-1</sup>. ATR-FTIR spectra were recorded on a Bruker TENSOR 27 from 600 to 4000 cm<sup>-1</sup> at a resolution of 2 cm<sup>-1</sup>, equipped with an attenuated total reflectance (ATR) device with a ZnSe crystal. Brunauer Emmett-Teller (BET) analyses were performed on Micromeritics ASAP 2460 using N<sub>2</sub>. The samples were degassed at 250 °C for 12 h before measurement. X-band electron paramagnetic resonance (EPR) spectra of DMPO-spin adducts were recorded on a Bruker E580 EPR at room temperature. Metal contents in metal-lignin complexes and catalysts were determined by inductively coupled plasma optical emission spectrometer (ICP-OES).

#### 2.4. Catalytic evaluation

In a typical reaction, benzyl alcohol (BA, 0.5 mmol) and Co SAs-N@C catalyst ( $n_{\text{Co}}/n_{\text{BA}} = 0.025$ ) were added into a Schlenk flask

containing 5 mL methanol. The vessel was vacuumed and flushed with O<sub>2</sub> for five times. Then, the reaction was proceeded at 60 °C under 1 bar O<sub>2</sub> (oxygen balloon) for specific reaction time. After reaction, the products were determined by HPLC and/or GC–MS using 0.05 mmol anisole as internal standard.

#### 2.5. Oxidative esterification of HMF to FDE by Co SAs-N@C

Initially, HMF was synthesized from fructose according to the method reported by Galkin and co-workers. [22] Oxidative esterification of HMF to dimethyl furan-2,5-dicarboxylate (FDE) over Co SAs-N@C was carried out in a 1000 mL three-neck flask. The reaction system contained 17 mmol HMF, 5 mol% Co SAs-N@C, and 200 mL methanol with bubbled O<sub>2</sub> at the flow rate of 100 mL/min. The mixture was stirred and refluxed for 12 h. After reaction, the catalyst was recycled by filtration using 0.45 μm of film and washed with 3 × 50 mL of methanol. All the filtrates were combined and concentrated to ~40 mL using a rotary evaporator (50 °C, -0.1 MPa). Finally, 2.59 g white needles of FDE with a purity of 99% was obtained via crystallization from the concentrated solution at -20 °C overnight, corresponding to 82.6% of isolated yield. In addition, the recycled Co SAs-N@C catalyst was successively washed with deionized water and methanol, and then regenerated at 500 °C for 1 h under argon protection. It was used for the next batches of reaction.

#### 2.6. Synthesis of polyethylene furanoate (PEF)

For the synthesis of PEF, 3.6 g FDE and 2.5 mL ethylene glycol (EG) were used for polymerization according to the method reported by Kuchero and coworkers. [23] Finally, 3.9 g PEF was obtained, corresponding to 99.4% of product yield.

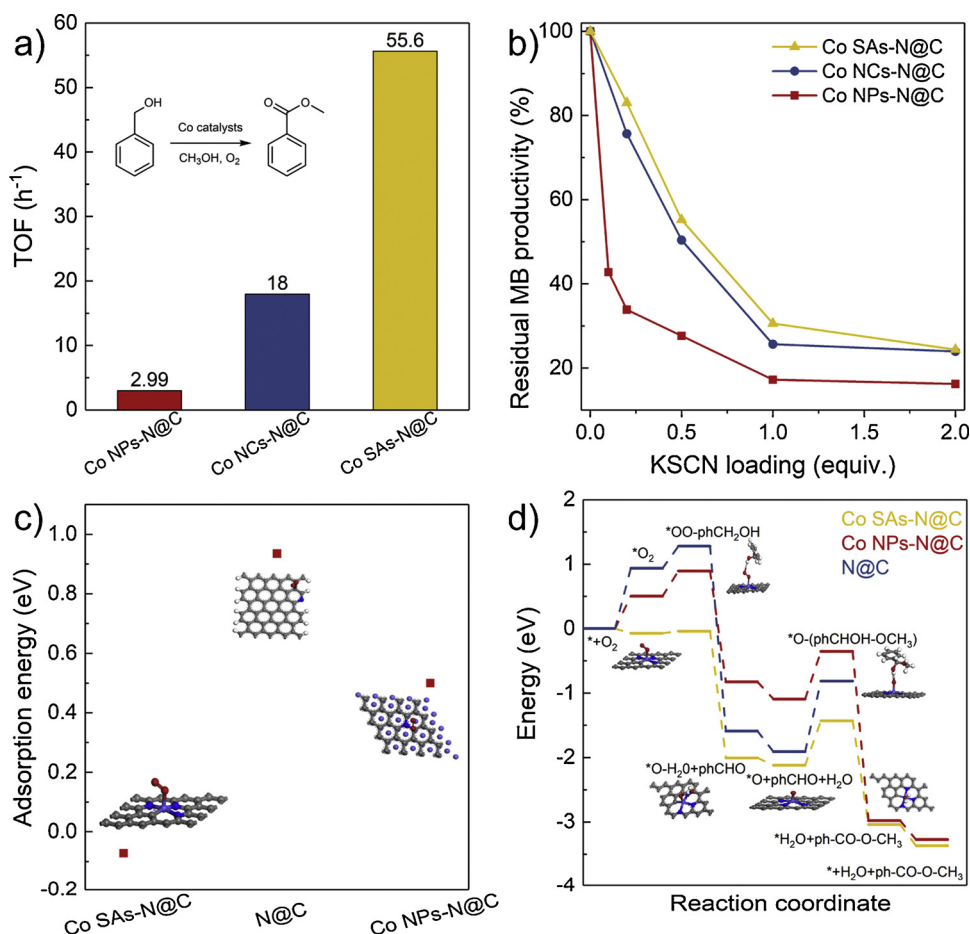


**Fig. 4.** Catalytic experiments and DFT calculations. a) Catalytic performances of Co catalysts, TOF values were calculated at 30% methyl benzoate (MB) yield. b) Titration experiments of active sites in Co catalysts with KSCN. c) The adsorption energy of  $\text{O}_2$  over catalysts. d) Energy profile and corresponding structures of oxidative esterification of benzyl alcohol catalyzed by catalysts.

### 3. Results and discussion

#### 3.1. Assembly of metal-lignin complexes

As shown in Fig. S1, lignin is a crosslinked phenolic polymer, primarily comprised of three substituted phenols through  $\beta$ -O-4 ether bonds and C-C linkages. The natural structure of lignin enables the assembly of metal-lignin (M-L) complexes as illustrated in Fig. 1a. In this strategy, metal ions act as nodes to coordinate multiple phenolic chain ends of lignin network to form insoluble supramolecular M-L complexes. The coordination interactions can hold the metal species in place during drying process. Additionally, the representative pictures reveal that the assembly process of M-L complexes is rapid and scalable by facile mixing of metal ions and lignin solution (Fig. S2a). In this way, other M-L complexes (e.g.  $\text{Fe}^{\text{III}}$ ,  $\text{Ni}^{\text{II}}$ ,  $\text{Cu}^{\text{II}}$ ,  $\text{Zn}^{\text{II}}$ ) and multiple metal-lignin hybrids can be prepared in a specific wide range of pH and enough metal loadings (Fig. S2b-g, S3). It can be seen in Fig. S4a, b, Zn and Co elements are homogeneously dispersed in granular Co/Zn-L complex. The coordination interactions in M-L complexes are confirmed by high resolution XPS and ATR-FTIR. As shown in Fig. S4d, the main peaks at 781.4 eV and 784.3 eV can be attributed to oxygen-coordinated Co ions. [24,25] Meanwhile, a new peak at  $646\text{ cm}^{-1}$  is observed in the ATR-FTIR spectra of Co-L and Co/Zn-L (Fig. S4e), which can be ascribed to the vibration of metal-oxygen bond. The results indicate the coordination interactions between metal ions and lignin. In addition, TGA analyses reveal that M-L complexes have high carbon yield (45%, Fig. S5) due to low oxygen content of lignin (~37 wt.%), higher than that of other biomass-derived phenols such as tannic acid (29%). [25]

#### 3.2. Preparation and characterization of SACs

The synthesis strategy of M SAs-N@C (M = Fe, Co, Ni, Cu) is demonstrated in Fig. 1b. Zn atoms are introduced into starting materials (M/Zn-L) to increase the spatial distance of targeted metal atoms, because Zn can be evaporated at high temperature ( $> 800\text{ }^\circ\text{C}$ ). [14] Di-cyandiamide is used as nitrogen source to incorporate N-species into carbon support to stabilize metal atoms (Fig. S6). For Co SAs-N@C catalyst, TEM and HAADF-STEM images confirm that isolated Co atoms are homogeneously dispersed on disordered carbon support (Fig. 1c-d). Owing to the facile assembly process of M-L complexes, gram scale production of Co SAs-N@C catalyst can be easily achieved in laboratory (Fig. S7).

The electronic structure of Co SAs-N@C catalyst was investigated by x-ray photoelectron spectroscopy (XPS), x-ray absorption near-edge structure (XANES), and extended x-ray absorption fine structure (EXAFS). As shown in Fig. 2a, the binding energy of the  $\text{Co}2\text{p}_{3/2}$  peak in Co SAs-N@C is at 780.5 eV, which is higher than that of  $\text{Co}^{\text{II}}$  (779.2 eV) but lower than that of  $\text{Co}^{\text{III}}$  (781 eV). [26] In addition, the XANES spectra and the peak of first derivative absorption spectra of Co SAs-N@C reveal that the energy of the absorption edge is located between that of CoO and  $\text{Co}_3\text{O}_4$  (Fig. 2b, c). These results indicate that the oxidation states of Co within Co SAs-N@C is between +2 and +3. [26] The EXAFS analysis further reveals that Co atoms are isolated and predominantly coordinated with N and/or C atoms in Co SAs-N@C (Fig. 2d). The best curve fitting of EXAFS data for Co SAs-N@C catalyst reveals a coordination number of 1.0 for C and 2.9 for N (Fig. 2d, Table 1).

To validate the applicability of our approach, Fe, Ni, and Cu based SACs were also prepared and characterized in the similar procedures. The metallic diffraction peaks are absent in the XRD patterns of all the

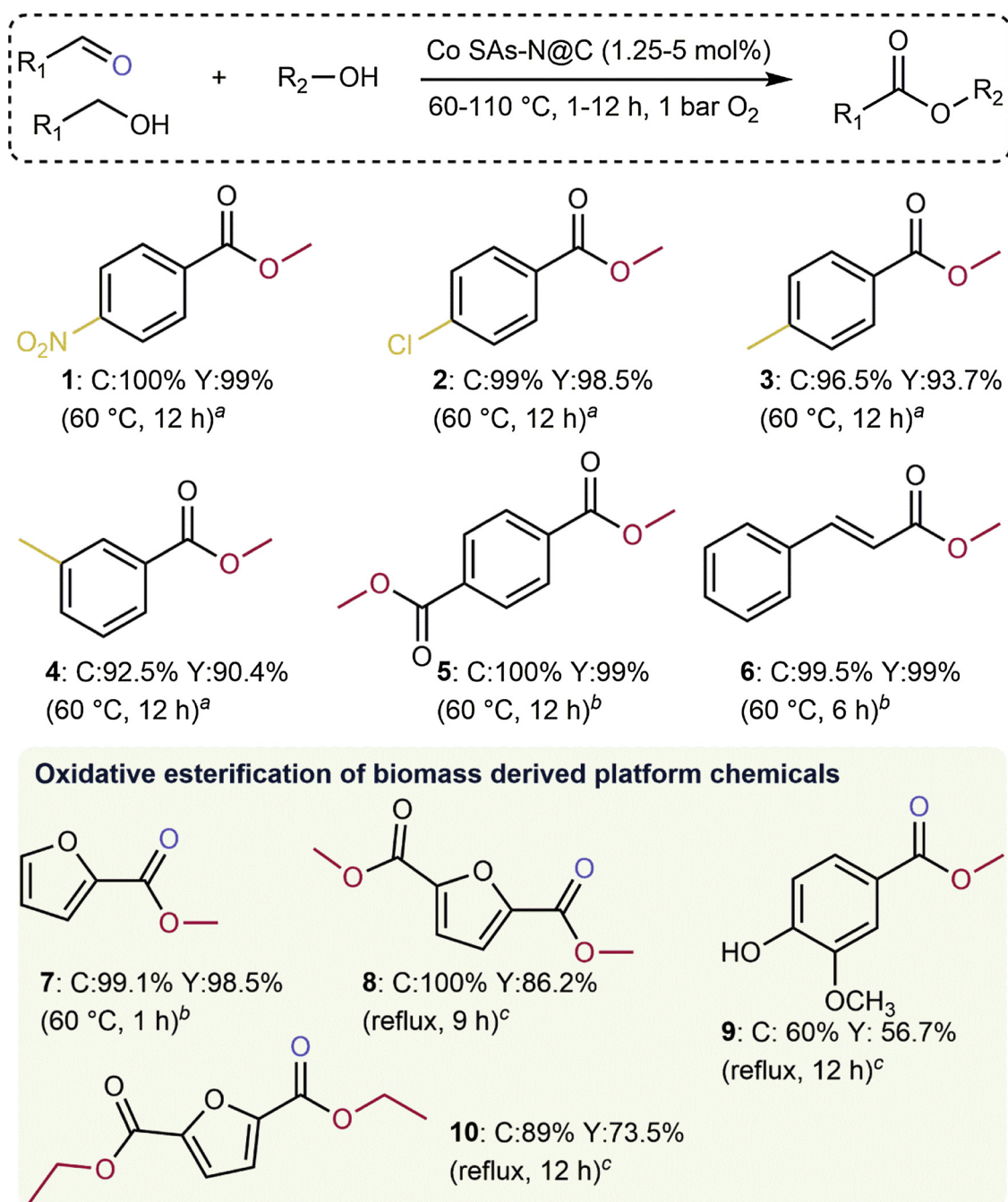


Fig. 5. Oxidative esterification of primary alcohols and aldehydes by Co SAs-N@C. C: conversion of substrate; Y: yield of ester product. <sup>a</sup>: 2.5 mol% of catalyst, <sup>b</sup>: 1.25 mol% of catalyst, <sup>c</sup>: 5 mol% of catalyst. The yield of 9–10 are isolated yield.

M SAs-N@C catalysts, indicating the well dispersion of metals (Fig. S8). As shown in Fig. 3, the HAADF-STEM images reveal the atomic dispersion of metal atoms in M SAs-N@C catalysts. Furthermore, the electronic structures of metal atoms in these catalysts were also identified by XANES and EXAFS (Fig. 3). The results confirm the prevalence of atomically dispersed M-N<sub>3</sub>C species in all M SAs-N@C samples (Table 1). Moreover, the composition of M SAs-N@C catalysts are summarized and depicted in Table S1.

### 3.3. Oxidative esterification of primary alcohol

The catalytic performances of M SAs-N@C catalysts were evaluated for aerobic oxidative esterification of primary alcohols, an important reaction for the production of fine chemicals and monomers of

polymers. [27,28] As shown in Table 2, only Co SAs-N@C catalyst exhibits reactivity for the selective methyl esterification of benzyl alcohol (BA) to give methyl benzoate (MB) with a high yield of 97.5%. On the contrary, Fe, Ni, Cu-based SACs show slight activity for the oxidation of BA into benzaldehyde. In accordance with the literatures, [27–29] Co is the only one of non-noble metal catalysts supported on N-doped carbon exhibited activity for oxidative esterification of alcohols. Nevertheless, there are few works to demonstrate the active sites of Co catalysts for this reaction. Cheng and co-workers speculated that highly dispersed CoN<sub>x</sub> species on carbon are responsible for the activity toward oxidative esterification. [29]

To further examine the active sites of Co SAs-N@C catalyst for this reaction, Co nanoparticles supported on carbon (Co NPs-C), N-doped carbon (N@C), Co nanoparticles supported on N-doped carbon (Co NPs-



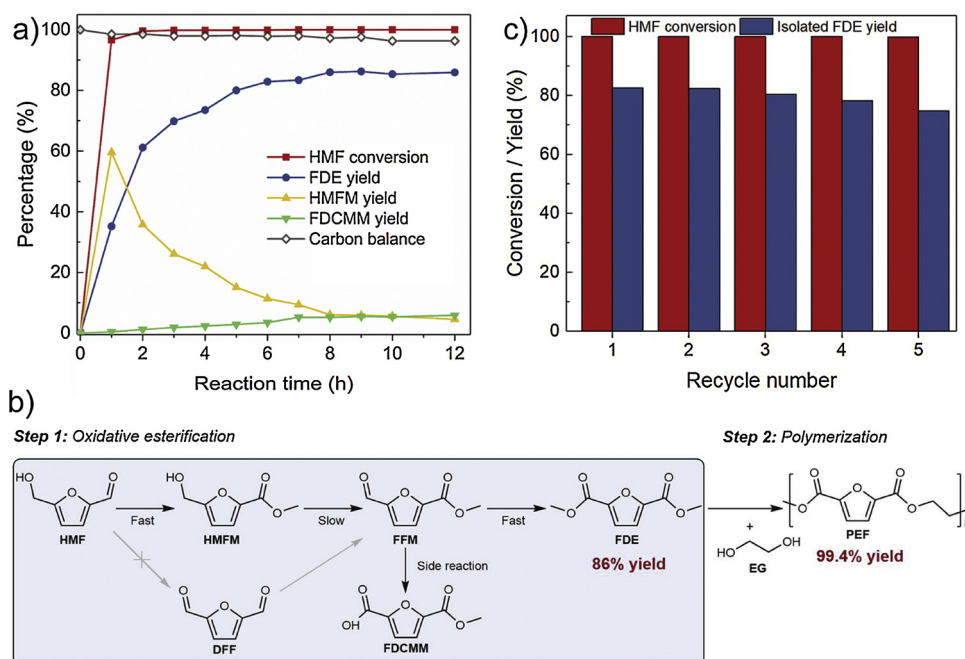


Fig. 6. a) Kinetic reaction of methyl esterification of HMF over Co SAs-N@C and b) proposed reaction pathway. c) Recyclability of Co SAs-N@C.

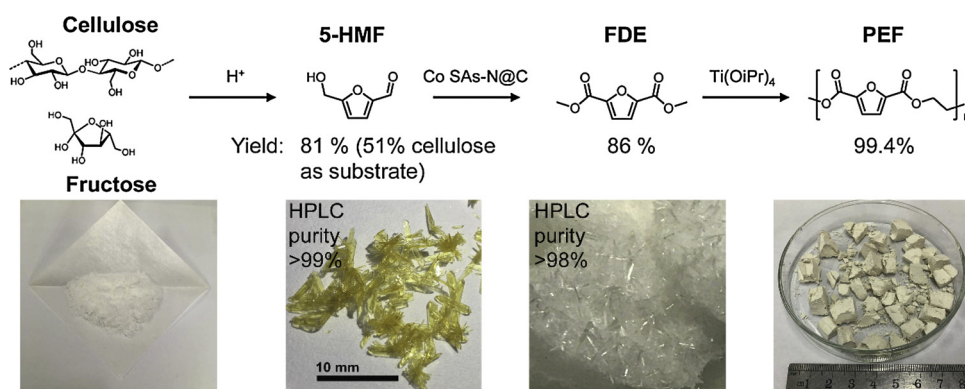


Fig. 7. Synthesis of PEF from C6 sugars.

N@C), and Co nanoclusters supported on N-doped carbon (Co NCs-N@C) were prepared and confirmed by TEM, XRD, XAFS, Raman spectroscopy, and N<sub>2</sub>-adsorption isotherm (Fig. S9-16). It can be seen in entry 1 of Table S2 that Co NPs-C is inactive for the transformation of BA. Meanwhile, 14.6% of benzaldehyde and only 0.6% of MB are produced from BA over N@C (entry 2, Table S2), suggesting that N-species on carbon are active for the oxidation of BA but sluggish to promote the esterification of benzaldehyde. Moreover, N-doped carbon supported Co catalysts (i.e. Co NPs-N@C, Co NCs-N@C, and Co SAs-N@C) can successfully trigger the oxidative esterification of BA (entries 3–7, Table S2). In detail, Co SAs-N@C catalyst give a turnover frequency (TOF) value of 55.6 h<sup>-1</sup>, which is 18.6 times over Co NPs-N@C (2.99 h<sup>-1</sup>) and 3 times over Co NCs-N@C (18 h<sup>-1</sup>), respectively (Fig. 4a and Fig. S17). In comparison with state-of-art catalysts (Fig. S18 and Table S3), the catalytic performance of Co SAs-N@C outperforms the reported non-noble metal heterogeneous catalysts, [27,28] most noble-metal based heterogeneous catalysts [30], and homogenous catalysts [31,32].

To investigate the active sites of N-doped carbon supported Co catalysts, titration experiments were conducted using KSCN to block the activity of metal-centred complexes (i.e. Co-N<sub>x</sub> population), while it does not impact the activity of large nanoparticles. [15,16] It can be seen in Fig. 4b, Co NPs-N@C dramatically losses 57% of its original MB

productivity after adding 0.1 equiv. KSCN owing to the poisoning of small quantity of Co-N<sub>x</sub> species. [33] On the contrary, for Co NCs-N@C and Co SAs-N@C catalysts, their catalytic activities present a nearly linear decrease with the increase of SCN<sup>-</sup> concentration at the initial stage (loading of SCN<sup>-</sup> < 1 equiv.). When the loading amount of SCN<sup>-</sup> exceeds 1.0 equiv., obvious decrease of the reactivity is not observed for all the Co catalysts. The residual MB productivity of the catalysts maybe attributed to the encapsulated Co NPs in graphitic carbon shells in Co NPs-N@C (Fig. S12b) and isolated Co atoms located in multiple graphitic layers (Fig. 1e). Our results further confirm the conjecture proposed by Cheng et al. [29] that the cobalt chelate complexes in the graphene lattice are dominant active sites for aerobic oxidative esterification.

The role of O<sub>2</sub> in this reaction was investigated by electron paramagnetic resonance (EPR) spectroscopy. As shown in Fig. S19, the typical signal of the adducts of superoxide radical anion (:O<sub>2</sub><sup>-</sup>) and DMPO are observed in the EPR spectra of N@C and N-doped carbon supported Co catalysts, hinting that incorporation of nitrogen heteroatoms into carbon can activate O<sub>2</sub> for initiating this reaction. It has been reported that N-species on carbon are capable of activating O<sub>2</sub> for oxygen reduction reaction [34] and epoxidation reaction [35]. In addition, the oxidative esterification of BA is significantly depressed in the absence of O<sub>2</sub> (entry 8 in Table S2), or adding butylated

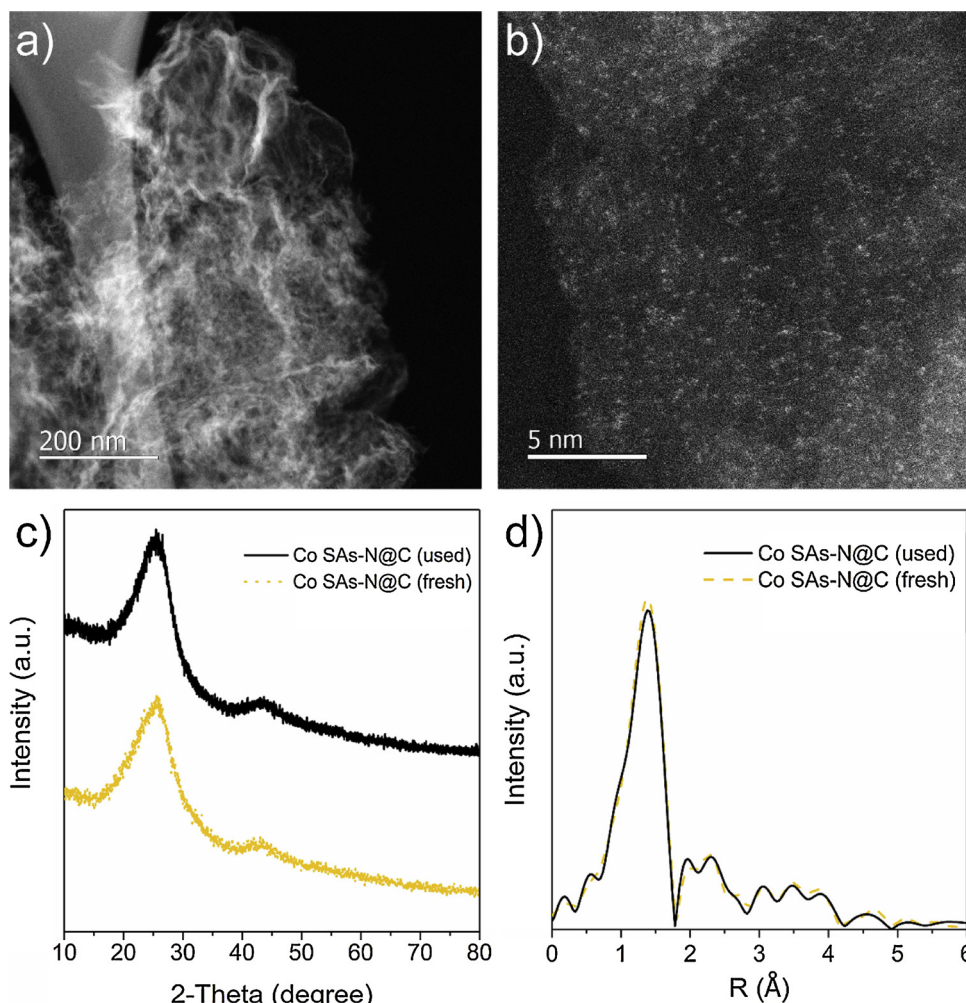


**Fig. 8.** Structural characterization of recycled Co SAs-N@C after 5 batches. a, b) HAADF-STEM images, c) XRD spectra, and d) EXAFS spectra of fresh and used Co SAs-N@C.

hydroxytoluene, a free-radical scavenger (entry 9 in Table S2), indicating reactive oxygen involved in this reaction.

Additionally, DFT calculations were further conducted to understand the catalytic mechanism of Co SAs-N@C for oxidative esterification reaction. Based on the XANES and EXAFS results, the optimized models of Co SAs-N@C, Co NPs-N@C, and N@C were built (Fig. S20). N-dopants will affect the local structure and electronic density of the central metal Co atom in Co SAs-N@C catalyst. The occupation of Co 3d under fermi level of Co SAs-N@C has lower electron density than DV-Co-C catalyst without N coordination (Fig. S21a). It would change the adsorption style of  $O_2$  from side-on (on DV-Co-C with the hirshfeld charge of -0.094 eV) to end-on (on Co SAs-N@C with the hirshfeld charge of -0.126 eV), leading to lower adsorption strength of  $O_2$  on Co SAs-N@C (Fig.S21b). There is a common idea that the aerobic oxidation reaction is always beginning with the activation of  $O_2$  [36]. It can be seen in Fig. 4c that the  $O_2$  adsorption energy of Co SAs-N@C (-0.07 eV) is much lower than that of Co NPs-N@C (0.5 eV) and N@C (0.94 eV). Then, the activated oxygen species are combining with BA and promote the dehydrogenative oxidation of BA to benzaldehyde, as evidenced by dynamic reactions (Fig. S17). As shown in Fig. 4d, DFT calculations reveal that the reaction energy barriers of BA activation to form benzaldehyde over Co SAs-N@C, Co NPs-N@C, and N@C are 0.1, 0.5, and 0.9 eV, respectively. In addition, DFT calculations show that the energy barriers of the formation of hemiacetal between benzaldehyde and methanol are 0.69, 0.74 and 1.1 eV for Co SAs-N@C, Co NPs-N@C, and N@C catalyst, respectively, suggesting that this step is the rate-

limiting step in this reaction. It is agreement with the dynamic reactions that benzaldehyde is the only detected intermediate (Fig. S17). Moreover, the result explains the fact that N@C is inactive for producing MB because of high energy barrier for the activation of benzaldehyde (Fig. 4d).

To investigate the applicability of Co SAs-N@C catalyst, we initially extend the substrate scope to substitute aromatic alcohols. As shown in 1–6 of Fig. 5, excellent yields (> 90%) of corresponding esters are obtained over the catalyst. In addition, the oxidative esterification of biomass-derived platform chemicals (i.e. furfural, HMF, and vanillin) were performed. As shown in 7–9 of Fig. 5, the corresponding methyl ester yields are 98.5%, 86.2% and 56.7% for furfural, HMF, and vanillin, respectively. The low yield of methyl vanillate may be attributed to the presence of phenol group in vanillin and methyl vanillate, which can scavenge radical species during the reaction. [37] Moreover, ethyl esterification of HMF also gives a good isolated yield of 73.5% (10 of Fig. 5). The methyl 2-furoate and methyl vanillate can be used as high value-added specialty fragrances, [38] while the corresponding esters of HMF are important building blocks for renewable plastics.

#### 3.4. Integrated biorefinery for renewable plastic

In the past decade, converting HMF into 2,5-furandicarboxylic acid (FDCA), [39–41] and then followed by esterification, transesterification, and polymerization to produce biomass-based polyester plastics is of significant economic and environmental profit [23,42]. In this



context, the directly oxidative esterification of HMF is attractive because of its higher step economy in comparison with the multiple reaction process. As a proof-of-concept, we performed the dynamic experiments for converting HMF into 2, 5-furandicarboxylic acid dimethyl ester (FDE) using Co SAs-N@C catalyst at gram scale. As shown in Fig. 6a, HMF is rapidly consumed and transformed to 5-hydroxymethyl-2-furoic acid methyl ester (HMFM) and FDE. The maximum yield of FDE (86%) is obtained after 9 h with a carbon balance of 97.6% and a productivity of 1.9 mol/mol<sub>cat.</sub>/h, surpassing all the reported heterogeneous Co-catalysts (Table S4). [43–45] Notably, 2, 5-diformylfuran (DFF) and 5-formyl-2-furoic acid methyl ester (FFM) are not detected during the reaction. Based on the results, a proposed reaction pathway for this reaction over Co SAs-N@C catalyst is shown in Fig. 6b. The FDE yield (86%) of this one-pot approach is higher than that of oxidation-esterification techniques (73%). [23] Moreover, the FDE product can be easily isolated from reacted solution through simple evaporation and crystallization, giving an isolation yield of 82.6% with high purity (> 98%). Based on this strategy, we demonstrate an integrated biorefinery that HMF is produced from biomass-derived C6 sugars via dehydration, then followed by one-pot oxidative esterification using lignin-based Co SAs-N@C catalyst to give FDE (Fig. 7). After a conventional polymerization of FDE and ethylene glycol (EG), high yield (99.4%) of PEF is obtained (Fig. 6b,7). Notably, EG can also be made from cellulose. [46] The structure of the HMF, FDE and PEF in the process are identified by NMR and/or ATR-FTIR techniques (Fig. S22–28). In addition, Co SAs-N@C catalyst can be easily recycled from the reaction system by filtration. After five batches of recycling, the HMF conversion and isolated yield of FDE remain 99.8% and 90% of fresh catalyst, respectively (Fig. 6c). Combined with HAADF-STEM, XRD, and XAFS techniques, the results indicate that Co SAs-N@C catalyst is stable under the reaction conditions (Fig. 8).

#### 4. Conclusion

In summary, we demonstrate a facile and robust metal-lignin coordination strategy for the scalable synthesis of SACs and full biomass utilization. The synthesis approach takes advantage of natural phenolic structure of lignin to spatially confine metal ions in metal-lignin complexes, opening a potentially advantageous route toward lignin valorization. Experiments and DFT calculations reveal that isolated Co-N<sub>3</sub>C moieties on N-doped carbon are responsible for the aerobic oxidative esterification of alcohols and aldehydes. Based on the findings, we demonstrate an integrated biorefinery, in which carbohydrates derived HMF and furfural are converted into valued esters by lignin-based Co SAs-N@C catalyst. Apart from biorefinery reactions, atomically dispersed metal catalysts are rising star for green synthesis of fine/bulk chemicals, [47,48] environmental remediation [2,49], photo/electrochemistry [50], etc.

#### Author contributions

Y.L. supervised this project and wrote the manuscript. H.Z. prepared the catalysts, performed the experiments and wrote the manuscript. S.H. performed HAADF-STEM analysis. H.X. and X.W. synthesized HMF. Z.J. and H.Z. conducted XAFS analysis. S.C. and Y.C. conducted DFT calculations.

#### Notes

The authors declare no conflict of interest.

#### Acknowledgments

This study was financially funded by the National Natural Science Foundation of China (NSFC, 21476016; 21776009), and Joint Fund of National Natural Science Foundation of China (U1732267). Also

acknowledged Dr. Tengfei Gao for helpful advice. Most of the calculations were conducted with the facilities at the Supercomputing Center of Wuhan University.

#### Appendix A. Supplementary data

Supplementary material related to this article can be found, in the online version, at doi:<https://doi.org/10.1016/j.apcatb.2019.117767>.

#### References

- [1] G. Malta, S.A. Kondrat, S.J. Freakley, C.J. Davies, L. Lu, S. Dawson, A. Thetford, E.K. Gibson, D.J. Morgan, W. Jones, P.P. Wells, P. Johnston, C.R. Catlow, C.J. Kiely, G.J. Hutchings, Identification of single-site gold catalysis in acetylene hydrochlorination, *Science* 355 (2017) 1399–1403.
- [2] H. Wang, J. Dong, L.F. Allard, S. Lee, S. Oh, J. Wang, W. Li, M. Shen, M. Yang, Single-site Pt/La-Al<sub>2</sub>O<sub>3</sub> stabilized by barium as an active and stable catalyst in purifying CO and C<sub>3</sub>H<sub>6</sub> emissions, *Appl. Catal. B-Environ.* 244 (2019) 327–339.
- [3] B. Qiao, A. Wang, X. Yang, L.F. Allard, Z. Jiang, Y. Cui, J. Liu, J. Li, T. Zhang, Single-atom catalysis of CO oxidation using Pt<sub>1</sub>/FeO<sub>x</sub>, *Nat. Chem.* 3 (2011) 634–641.
- [4] H.T. Chung, D.A. Cullen, D. Higgins, B.T. Sneed, E.F. Holby, K.L. More, P. Zelenay, Direct atomic-level insight into the active sites of a high-performance PGM-free ORR catalyst, *Science* 357 (2017) 479–484.
- [5] K. Liu, Z. Qiao, S. Hwang, Z. Liu, H. Zhang, D. Su, H. Xu, G. Wu, G. Wang, Mn- and N-doped carbon as promising catalysts for oxygen reduction reaction: theoretical prediction and experimental validation, *Appl. Catal. B-Environ.* 243 (2019) 195–203.
- [6] Z. Geng, Y. Cao, W. Chen, X. Kong, Y. Liu, T. Yao, Y. Lin, Regulating the coordination environment of Co single atoms for achieving efficient electrocatalytic activity in CO<sub>2</sub> reduction, *Appl. Catal. B-Environ.* 240 (2019) 234–240.
- [7] D. Deng, X. Chen, L. Yu, X. Wu, Q. Liu, Y. Liu, H. Yang, H. Tian, Y. Hu, P. Du, A single iron site confined in a graphene matrix for the catalytic oxidation of benzene at room temperature, *Sci. Adv.* 1 (2015) e1500462.
- [8] S.K. Kaiser, R. Lin, S. Mitchell, E. Fako, F. Krumeich, R. Hauert, O.V. Safonova, V.A. Kondratenko, E.V. Kondratenko, S.M. Collins, P.A. Midgley, N. López, J. Pérez-Ramírez, Controlling the speciation and reactivity of carbon-supported gold nanostructures for catalysed acetylene hydrochlorination, *Chem. Sci.* 10 (2019) 359–369.
- [9] X. Li, X. Huang, S. Xi, S. Miao, J. Ding, W. Cai, S. Liu, X. Yang, H. Yang, J. Gao, J. Wang, Y. Huang, T. Zhang, B. Liu, Single cobalt atoms anchored on porous N-doped graphene with dual reaction sites for efficient fenton-like catalysis, *J. Am. Chem. Soc.* 140 (2018) 12469–12475.
- [10] X.F. Yang, A. Wang, B. Qiao, J. Li, J. Liu, T. Zhang, Single-atom catalysts: a new frontier in heterogeneous catalysis, *Acc. Chem. Res.* 46 (2013) 1740–1748.
- [11] C. Rivera-Cárcamo, P. Serp, Single atom catalysts on carbon-supported gold, *ChemCatChem* 10 (2018) 5058–5091.
- [12] J. Liu, Catalysis by supported single metal atoms, *ACS Catal.* 7 (2016) 34–59.
- [13] A. Wong, Q. Liu, S. Griffin, A. Nicholls, J.R. Regalbutto, Synthesis of ultrasmall, homogeneously alloyed, bimetallic nanoparticles on silica supports, *Science* 358 (2017) 1427–1430.
- [14] P. Yin, T. Yao, Y. Wu, L. Zheng, Y. Lin, W. Liu, H. Ju, J. Zhu, X. Hong, Z. Deng, G. Zhou, S. Wei, Y. Li, Single cobalt atoms with precise N-coordination as superior oxygen reduction reaction catalysts, *Angew. Chem. Int. Ed.* 55 (2016) 10800–10805.
- [15] C. Tang, A.E. Surkus, F. Chen, M.M. Pohl, G. Agostini, M. Schneider, H. Junge, M. Beller, A stable nanocobalt catalyst with highly dispersed Co<sub>N</sub> active sites for the selective dehydrogenation of formic acid, *Angew. Chem. Int. Ed.* 56 (2017) 16616–16620.
- [16] W. Liu, L. Zhang, X. Liu, X. Yang, S. Miao, W. Wang, A. Wang, T. Zhang, Discriminating catalytically active Fe<sub>N</sub> species of atomically dispersed Fe-N-C catalyst for selective oxidation of the C-H bond, *J. Am. Chem. Soc.* 139 (2017) 10790–10798.
- [17] P. Liu, Y. Zhao, R. Qin, S. Mo, G. Chen, L. Gu, D.M. Chevrier, P. Zhang, Q. Guo, D. Zang, B. Wu, G. Fu, N. Zheng, Photochemical route for synthesizing atomically dispersed palladium catalysts, *Science* 352 (2016) 797–801.
- [18] T. Zheng, K. Jiang, N. Ta, Y. Hu, J. Zeng, J. Liu, H. Wang, Large-scale and highly selective CO<sub>2</sub> electrocatalytic reduction on nickel single-atom catalyst, *Joule* 3 (2019) 265–278.
- [19] Y. Li, B. Chen, X. Duan, S. Chen, D. Liu, K. Zang, R. Si, F. Lou, X. Wang, M. Rønning, L. Song, J. Luo, D. Chen, Atomically dispersed Fe-N-P-C complex electrocatalysts for superior oxygen reduction, *Appl. Catal. B-Environ.* 249 (2019) 306–315.
- [20] Emmanouela Filippidi, Thomas R. Cristiani, Claus D. Eisenbach, J. Herbert Waite, Jacob N. Israelachvili, B. Kollbe Ahn, M.T. Valentine, Toughening elastomers using mussel-inspired iron-catechol complexes, *Science* 358 (2017) 502–505.
- [21] H. Zhou, H. Xu, Y. Liu, Aerobic oxidation of 5-hydroxymethylfurfural to 2,5-furandicarboxylic acid over Co/Mn-lignin coordination complexes-derived catalysts, *Appl. Catal. B-Environ.* 244 (2019) 965–973.
- [22] K.I. Galkin, E.A. Krivodaeva, L.V. Romashov, S.S. Zaleskiy, V.V. Kachala, J.V. Burykina, V.P. Ananikov, Critical influence of 5-hydroxymethylfurfural aging and decomposition on the utility of biomass conversion in organic synthesis, *Angew. Chem. Int. Ed.* 55 (2016) 8338–8342.
- [23] F.A. Kucherov, E.G. Gordeev, A.S. Kashin, V.P. Ananikov, Three-dimensional

- printing with biomass-derived PEF for carbon-neutral manufacturing, *Angew. Chem. Int. Ed.* 56 (2017) 15931–15935.
- [24] X. Wang, L.L. Lu, Z.L. Yu, X.W. Xu, Y.R. Zheng, S.H. Yu, Scalable template synthesis of resorcinol-formaldehyde/graphene oxide composite aerogels with tunable densities and mechanical properties, *Angew. Chem. Int. Ed.* 54 (2015) 2397–2401.
- [25] J. Wei, Y. Liang, Y. Hu, B. Kong, J. Zhang, Q. Gu, Y. Tong, X. Wang, S.P. Jiang, H. Wang, Hydrothermal synthesis of metal-polyphenol coordination crystals and their derived metal/N-doped carbon composites for oxygen electrocatalysis, *Angew. Chem. Int. Ed.* 55 (2016) 12470–12474.
- [26] Y. Pan, R. Lin, Y. Chen, S. Liu, W. Zhu, X. Cao, W. Chen, K. Wu, W.C. Cheong, Y. Wang, L. Zheng, J. Luo, Y. Lin, Y. Liu, C. Liu, J. Li, Q. Lu, X. Chen, D. Wang, Q. Peng, C. Chen, Y. Li, Design of single-atom Co-N<sub>5</sub> catalytic site: a robust electrocatalyst for CO<sub>2</sub> reduction with nearly 100% CO selectivity and remarkable stability, *J. Am. Chem. Soc.* 140 (2018) 4218–4221.
- [27] R.V. Jagadeesh, H. Junge, M.M. Pohl, J. Radnik, A. Bruckner, M. Beller, Selective oxidation of alcohols to esters using heterogeneous Co<sub>3</sub>O<sub>4</sub>-N@C catalysts under mild conditions, *J. Am. Chem. Soc.* 135 (2013) 10776–10782.
- [28] H. Su, K.X. Zhang, B. Zhang, H.H. Wang, Q.Y. Yu, X.H. Li, M. Antonietti, J.S. Chen, Activating cobalt nanoparticles via the Mott-Schottky effect in nitrogen-rich carbon shells for base-free aerobic oxidation of alcohols to esters, *J. Am. Chem. Soc.* 139 (2017) 811–818.
- [29] T. Cheng, H. Yu, F. Peng, H. Wang, B. Zhang, D. Su, Identifying active sites of CoNC/CNT from pyrolysis of molecularly defined complexes for oxidative esterification and hydrogenation reactions, *Catal. Sci. Technol.* 6 (2016) 1007–1015.
- [30] L.L. Chng, J. Yang, J.Y. Ying, Efficient synthesis of amides and esters from alcohols under aerobic ambient conditions catalyzed by a Au/mesoporous Al<sub>2</sub>O<sub>3</sub> nanocatalyst, *ChemSusChem* 8 (2015) 1916–1925.
- [31] S. Gowrisankar, H. Neumann, M. Beller, General and selective palladium-catalyzed oxidative esterification of alcohols, *Angew. Chem. Int. Ed.* 50 (2011) 5139–5143.
- [32] C. Liu, J. Wang, L. Meng, Y. Deng, Y. Li, A. Lei, Palladium-catalyzed aerobic oxidative direct esterification of alcohols, *Angew. Chem. Int. Ed.* 50 (2011) 5144–5148.
- [33] R.V. Jagadeesh, K. Murugesan, A.S. Alshammari, H. Neumann, M.M. Pohl, J. Radnik, M. Beller, MOF-derived cobalt nanoparticles catalyze a general synthesis of amines, *Science* 358 (2017) 326–332.
- [34] H.B. Yang, J. Miao, S.F. Hung, J. Chen, H.B. Tao, X. Wang, L. Zhang, R. Chen, J. Gao, H.M. Chen, L. Dai, B. Liu, Identification of catalytic sites for oxygen reduction and oxygen evolution in N-doped graphene materials: development of highly efficient metal-free bifunctional electrocatalyst, *Sci. Adv.* 2 (2016) e1501122.
- [35] G. Wen, Q. Gu, Y. Liu, R. Schlögl, C. Wang, Z. Tian, D.S. Su, Biomass-derived graphene-like carbon: efficient metal-free carbocatalysts for epoxidation, *Angew. Chem. Int. Ed.* 57 (2018) 16898–16902.
- [36] B. Qiao, T. Li, F. Liu, Y. Tang, L. Li, S. Miao, Y. Su, J. Zhang, J. Huang, H. Sun, M. Haruta, A. Wang, J. Li, T. Zhang, Maximizing interfacial sites by single-atom catalyst for solvent-free selective oxidation of primary alcohol, *Angew. Chem. Int. Ed.* 57 (2018) 7795–7799.
- [37] Y. Ma, K. Chen, J. Ma, G. Xu, S. Dong, B. Chen, J. Li, Z. Chen, X. Zhou, G. Cui, A biomass based free radical scavenger binder endowing a compatible cathode interface for 5 V lithium-ion batteries, *Energy Environ. Sci.* 12 (2019) 273–280.
- [38] M. Signorello, F. Menegazzo, L. Contessotto, F. Pinna, M. Manzoli, F. Boccuzzi, Au/ZrO<sub>2</sub>: an efficient and reusable catalyst for the oxidative esterification of renewable furfural, *Appl. Catal. B-Environ.* 129 (2013) 287–293.
- [39] A.H. Motagamwala, W.Y. Won, C. Sener, D.M. Alonso, C.T. Maravelias, J.A. Dumesic, Toward biomass-derived renewable plastics: production of 2,5-furandicarboxylic acid from fructose, *Sci. Adv.* 4 (2018) eaap9722.
- [40] Z. Zhang, G.W. Huber, Catalytic oxidation of carbohydrates into organic acids and furan chemicals, *Chem. Soc. Rev.* 47 (2018) 1351–1390.
- [41] B.J. Taitt, D.-H. Nam, K.-S. Choi, A comparative study of nickel, cobalt, and iron oxyhydroxide anodes for the electrochemical oxidation of 5-hydroxymethylfurfural to 2,5-furandicarboxylic acid, *ACS Catal.* 9 (2018) 660–670.
- [42] A.J.J.E. Eerhart, A.P.C. Faaij, M.K. Patel, Replacing fossil based PET with biobased PEF; process analysis, energy and GHG balance, *Energy Environ. Sci.* 5 (2012) 6407–6422.
- [43] Y. Sun, H. Ma, X. Jia, J. Ma, Y. Luo, J. Gao, J. Xu, A high-performance base-metal approach for the oxidative esterification of 5-hydroxymethylfurfural, *ChemCatChem* 8 (2016) 2907–2911.
- [44] J. Deng, H.J. Song, M.S. Cui, Y.P. Du, Y. Fu, Aerobic oxidation of hydroxymethylfurfural and furfural by using heterogeneous Co<sub>x</sub>O<sub>y</sub>-N@C catalysts, *ChemSusChem* 7 (2014) 3334–3340.
- [45] F. Li, X.L. Li, C. Li, J. Shi, Y. Fu, Aerobic oxidative esterification of 5-hydroxymethylfurfural to dimethyl furan-2,5-dicarboxylate by using homogeneous and heterogeneous PdCoBi/C catalysts under atmospheric oxygen, *Green Chem.* 20 (2018) 3050–3058.
- [46] W. Liu, Y. Chen, H. Qi, L. Zhang, W. Yan, X. Liu, X. Yang, S. Miao, W. Wang, C. Liu, A. Wang, J. Li, T. Zhang, A durable nickel single-atom catalyst for hydrogenation reactions and cellulose valorization under harsh conditions, *Angew. Chem. Int. Ed.* 57 (2018) 7071–7075.
- [47] L. Zhang, Y. Ren, W. Liu, A. Wang, T. Zhang, Single-atom catalyst: a rising star for green synthesis of fine chemicals, *Sci. Rev.* 5 (2018) 653–672.
- [48] Z. Chen, E. Vorobyeva, S. Mitchell, E. Fako, M.A. Ortuño, N. López, S.M. Collins, P.A. Midgley, S. Richard, G. Vilé, J. Pérez-Ramírez, A heterogeneous single-atom palladium catalyst surpassing homogeneous systems for Suzuki coupling, *Nat. Nanotechnol.* 13 (2018) 702–707.
- [49] K. Yang, Y.X. Liu, J.G. Deng, X.T. Zhao, J. Yang, Z. Han, Z.Q. Hou, H.X. Dai, Three-dimensionally ordered mesoporous iron oxide-supported single-atom platinum: highly active catalysts for benzene combustion, *Appl. Catal. B-Environ.* 244 (2019) 650–659.
- [50] L. Jiao, H.-L. Jiang, Metal-organic-framework-based single-atom catalysts for energy applications, *Chemistry* (2019), <https://doi.org/10.1016/j.chempr.2018.1012.1011>.